State estimation and inverse problems in electrical impedance tomography: observability, convergence and regularization

2015 Inverse Problems 31 045004

(http://iopscience.iop.org/0266-5611/31/4/045004)

IOP Publishing Inverse Problems
Inverse Problems 31 (2015) 045004 (27pp) doi:10.1088/0266-5611/31/4/045004

State estimation and inverse problems in electrical impedance tomography: observability, convergence and regularization

D Sbarbaro[1,4], M Vauhkonen[2] and T A Johansen[3]

[1] Department of Electrical Engineering, Universidad de Concepcion, Concepcion, Chile
[2] Department of Applied Physics, University of Eastern Finland, Finland
[3] Department of Engineering Cybernetics, Center for Autonomous Marine Operations and Systems, NTNU, Trondheim, Norway

E-mail: daniel.sbarbaro@udec.cl, marko.vauhkonen@uef.fi and Tor.Arne.Johansen@itk.ntnu.no

Received 10 August 2014, revised 24 January 2015
Accepted for publication 16 February 2015
Published 10 March 2015

Abstract

Solving electrical impedance tomography (EIT) inverse problems in real-time is a challenging task due to their dimension, the nonlinearities involved and the fact that they are ill-posed. Thus, efficient algorithms are required to address the application of tomographic technologies in process industry. In practical applications the EIT inverse problem is often linearized for fast and robust reconstruction. The aim of this paper is to analyse the solution of linearized EIT inverse problem from the perspective of a state estimation problem, providing links between regularization, observability and convergence of the algorithms. In addition, also a new way to define the fictitious outputs is proposed, leading to observers with fewer parameters than with the approach widely used in literature. Simulation of EIT examples illustrate the main ideas and algorithmic improvements of the proposed approaches.

Keywords: State estimation, inverse problems, electrical impedance tomography

1. Introduction

The real-time solution of inverse problems, such as in electrical impedance tomography (EIT), is very important in many practical industrial applications. In EIT the aim is to estimate

[4] Author to whom any correspondence should be addressed.

a set of unknown variables representing some characteristic of the material (conductivity or resistivity) in a region of interest, given a set of measurements at the boundary (voltages). This problem is ill-posed and some regularization methods are normally used to solve it [23, 32].

In static imaging case it is possible to use a full set of independent current patterns and the corresponding voltages for each image and Newton–Raphson type methods provide good performance in terms of convergence rate and residual error [35]. However, in real-time applications the static techniques often do not provide satisfactory results due to the fast changes in the unknown variables. The information on their temporal evolution is lost or severely affected.

In the time-varying case, the reconstruction approach to solve the inverse problem can be formulated as a state estimation problem and the time-varying variables have been estimated, for example, with the aid of the Kalman filter [31] or extended Kalman filter (EKF) [17, 18, 28]. The use of unscented Kalman filters have also been proposed to deal with the non-linear characteristics of the problem [10, 15]. In order to deal with the computational complexity, reduced-order representations for the state variable have been proposed [33] . The estimation of region boundaries has also been carried out by Kalman filters [16, 19], extended Kalman filters [30] and unscented Kalman filters [11, 15]. The automated segmentation of EIT images by means of the Kalman filter has been proposed by [36].

Due to the the ill-posedness of the problem the image reconstruction procedure has to be regularized. One common option is to augment the output by adding fictitious outputs as suggested in [14]. This approach has been very successful in tackling many problems, but as far as we know there are no works addressing the system theoretical properties of this particular choice.

The need of having efficient and robust algorithms that can meet the requirement for real-time implementations; i.e. guaranteed performance, small number of mathematical operations and boundeness of all variables, leads us to consider the applications of deterministic observers, which are computationally simpler than recursive stochastic filters.

A state observer provides estimates of the internal state of a given system, from measurements of its input and output variables. The theory of state estimation is a well established field for both linear [20] and nonlinear dynamical systems [3]. The design of the observers based on the minimization of a cost function considering noise characteristics lead to recursive estimation algorithms; i.e. Kalman filters [4, 13]. Recent extensions of this approach, as described for instance in [27], deal with nonlinear systems and robustness issues.

Thus the main objective of this work is to analyze from an observer perspective the solution of the inverse problem, linking the algorithms with system's theoretical properties such as observability and convergence.

To focus the work on the properties of the algorithms and their relationship with the structure of the inverse problem only deterministic linear problems are addressed. However, the results can also be extended to the analysis of uncertain linear and non-linear models.

This paper is organized as follows: section 2 describes the EIT inverse problem to be addressed in this work. Section 3 provides a brief summary of known results concerning system properties required to have a well posed estimation problem and also observer design methods. In section 4, analysis of regularization strategies in the context of the observer design is carried out. Section 5 provides EIT examples to illustrate the main issues addressed in this paper. Finally in section 6 some conclusions and future work are addressed.

2. EIT inverse problem

The EIT model considers an object $\Omega \in R^2$ with a given a resistivity distribution ρ. The electrical currents i_j are injected into the object Ω through electrodes having a surface e_j located on the boundary $\partial\Omega$. The induced electrical potential u and the voltages v_j can be uniquely determined by solving the following partial differential equations representing the complete electrode model:

$$\nabla\left(\rho^{-1}\nabla u\right) = 0 \text{ in } \Omega \tag{1}$$

$$u + z_j\rho^{-1}\frac{\partial u}{\partial r} = v_j \text{ on } e_j, \quad j = 1, 2, \ldots, l \tag{2}$$

$$\int_{e_j} \rho^{-1}\frac{\partial u}{\partial r}\mathrm{d}s = i_j \quad j = 1, 2, \ldots, l \tag{3}$$

$$\frac{\partial u}{\partial r} = 0 \text{ on } \partial\Omega\backslash\bigcup_{j=1}^{l} e_j \tag{4}$$

where r is the outward unit normal, z_j is the effective contact impedance between the jth electrode and the surface and l is the total number of electrodes. In addition, the following two conditions taking into account the conservation of electrical charge and the selection of the ground electrode, respectively, are needed

$$\sum_{j=1}^{l} i_j = 0 \tag{5}$$

$$\sum_{j=1}^{l} v_j = 0 \tag{6}$$

The numerical solution of this model can be obtained using the finite element method (FEM). The potential at each node are calculated by the following linear matrix equation representing the finite element discretization of equations (1)–(6)

$$G(\rho)U_e = I_c \tag{7}$$

where $G(\rho) \in R^{(n+l-1)\times(n+l-1)}$ is a sparse block matrix, $U_e = [\alpha, \beta]^T \in R^{n+l-1}$, with α and β being vectors with the coefficient associated with the FEM model for the potentials and referenced voltages, $I_c \in R^{n+l-1}$ is a vector depending of the injected currents and n is the number of FEM nodes. The computed voltages for a given current pattern m; i.e. I_m, can be obtained by solving (7) for the potential on the electrodes guaranteeing equation (6) as follows

$$V_m = C\beta = CR(\rho)C^T I_m \tag{8}$$

where $V_m = [v_{1,m}, \ldots, v_{l,m}]^T$, $I_m = [i_{1,m}, \ldots, i_{l,m}]^T$ is a vector of injected currents, $R(\rho) \in R^{(l-1)\times(l-1)}$ is a block $(G^{-1})_{jk}$, $n+1 \leqslant j, k \leqslant n+l-1$ of the inverse matrix $G(\rho)^{-1}$ and $C \in R^{l\times(l-1)}$ is a sparse matrix [32]. Thus for M current patterns $V^M = [V_1^T, \ldots V_M^T]^T \in R^{Ml}$.

The evolution of $\rho(t)$ is described by a discrete-time model (state-equation)

$$\rho(t+1) = A\rho(t) + Bu(t) + \omega(t) \tag{9}$$

where $u(t) \in R^m$ is a vector of known external signals, $\omega(t) \in R^n$ is a random variable representing the state noise, $B \in R^{n\times m}$ the input matrix and $A \in R^{n\times n}$ is the state transition matrix. The deterministic external signals, $u(t)$, drive the dynamic of the resistivity fields. They may represent, for instance, point sources that can be manipulated in order to control some features of the resistivity field as described in [22, 24–26].

A linearized observation model (8) can be obtained by expanding V^M around ρ_0 and taking the first terms of the Taylor expansion

$$V^M - V^M(\rho_0) = \frac{\partial V^M(\rho)}{\partial \rho}\Big|_{\rho_0}(\rho - \rho_0) + \delta(\rho, \rho_0), \tag{10}$$

where $\delta(\rho, \rho_0)$ represents the higher order terms associated to the Taylor expansion, and

$$\frac{\|\delta(\rho, \rho_0)\|}{\|\rho - \rho_0\|} \to 0, \quad \text{as} \quad \|\rho - \rho_0\| \to 0. \tag{11}$$

Let us assume a neighborhood of ρ_0 such so that $\delta(\rho, \rho_0) \approx 0$ and the first term provides a reasonable approximation. By defining $x = \rho$, $y = V^M - V^M(\rho_0) + \frac{\partial V^M(\rho)}{\partial \rho}\Big|_{\rho_0}\rho_0$ and $C = \frac{\partial V^M(\rho)}{\partial \rho}\Big|_{\rho_0}$, equations (9) and (10) can be written as

$$\begin{aligned} x(t+1) &= Ax(t) + Bu(t) + \omega(t), \quad \text{with } x(0) = x_0 \text{ unknown} \\ y(t) &= Cx(t) + \nu(t) \end{aligned} \tag{12}$$

where $y(t) \in R^{Ml}$, $\nu(t) \in R^l$ represents the measurement noise, and $C \in R^{Ml\times n}$. Both state and measurement noises are assumed to have zero mean Gaussian distributions.

3. Observability, design and convergence: preliminaries

In order to estimate the resistivity given the measured voltages, the model (12) must satisfy certain system properties which will be summarized in this section.

3.1. System properties

Definition : Observability [2]. The invariant discrete linear system (12) is observable if $x(0)$ can be determined exactly from the zero input response $\{y(t),\ t \geqslant 1\}$.

The zero input response is characterized by setting the inputs to the system to zero:

$$\begin{aligned} x(t+1) &= Ax(t), \quad \text{with } x(0) = x_0 \text{ unknown} \\ y(t) &= Cx(t) \end{aligned} \tag{13}$$

Thus, the observability of system (12) is determined by the pair (A, C).

Theorem. *The pair (A, C) is observable if and only if the observability matrix $\mathcal{O}$ has rank equal to n, where*

$$\mathcal{O} = \begin{bmatrix} C^T & A^T C^T & \cdots & A^{n-1^T} C^T \end{bmatrix} \tag{14}$$

This result can be obtained by using the system equations to express the value of $x(0)$ in terms of n past values of $y(t)$ and $u(t)$. If the Observability matrix has full row rank, then $x(0)$

can be obtained by inverting $\mathcal{O}$. However, if the system is not observable, then $x(0)$ can not be estimated no matter the number of measurements taken.

Definition : Reachability [2]. The invariant discrete linear system (12) is reachable if, for every state $x(t)$, there is an input sequence $\{u(t),\ t \geqslant 1\}$ that drives the system from $x(0)$ to a state $x(t)$.

The reachability of system (12) is determined by the pair (A, B).

Theorem. *The pair (A, B) is reachable if and only if the reachability matrix $\mathcal{R}$ has rank equal to n, where*

$$\mathcal{R} = \begin{bmatrix} B & AB & \cdots & A^{n-1}B \end{bmatrix} \tag{15}$$

The proof of this result is based on successive substitutions of the system equations to express $x(n)$ in terms of an initial state and the control inputs up to time $n - 1$. If the system is uncontrollable, then there will be no inputs that can drive all the states to a desired position, either to zero state or to a trajectory.

These two structural properties play an important role in the design of estimation algorithms. If a system is not observable, then it will be impossible to design an algorithm with a prescribed dynamic to estimate the full state of the system.

3.2. Observers

The classical observer structure for estimating $x(t)$ of system (12) can be described by

$$\begin{aligned} \hat{x}(t+1) &= A\hat{x}(t) + Bu(t) + K\left(y - \hat{y}(t)\right) \\ \hat{y}(t) &= C\hat{x}(t) \end{aligned} \tag{16}$$

where $K \in R^{n \times Ml}$ is the observer gain [2]. Since the structure of the observer is defined, the observer design problem is reduced to find a gain K so that certain specifications in terms of stability, robustness and performance are satisfied.

The error dynamic depends on the eigenvalues of $A + KC$, and the design of the observer gain can be carried out by several methods: Pole placement, Lyapunov design, or optimization methods [5].

Optimal observer design considers the following cost function

$$I(\infty) = \frac{1}{2}\sum_{k=0}^{\infty} \| y(k) - C\hat{x}(k) \|^2_{N^{-1}} + \| \hat{x}(k+1) - A\hat{x}(k) - Bu(k) \|^2_{Q^{-1}} \tag{17}$$

where N and Q are symmetric positive definite matrices. The minimization of (17) with respect to $\hat{x}(k)$ subject to (12) is given by the following equations

$$\hat{x}(t+1) = A\hat{x}(t) + Bu(t) + K\left(y(t) - C\hat{x}(t)\right) \tag{18}$$

$$K = -\left(CPC^T + N\right)^{-1} CPA^T \tag{19}$$

$$APA^T - P + Q - APC^T\left(CPC^T + N\right)^{-1} CPA^T = 0 \tag{20}$$

The positive definite matrix P can be obtained by solving equation (20). This equation represents an algebraic Ricatti equation which can be solved, for instance, by using the MATLAB control system toolbox function *dare*. Additional numerical tools are described in [7] and [6].

3.3. Kalman filter

In addition, it is also possible to solve the problem based on all the measurements taken up to time t. The estimates are obtained by minimizing the cost function (21) subject to the observation and evolution models (12) [29]

$$I(t) = \frac{1}{2}\left[\| x(0) - \hat{x}(0) \|^2_{M^{-1}} + \sum_{k=0}^{t} \| y(k) - C\hat{x}(k) \|^2_{N^{-1}} + \| \hat{x}(k+1) - A\hat{x}(k) - Bu(k) \|^2_{Q^{-1}} \right] \tag{21}$$

where M^{-1}, N^{-1} and Q^{-1} are positive definite and symmetric matrices. The solution to the minimization problem can be written in terms of a set of recursive equations known as deterministic Kalman filter.

$$\begin{aligned} \hat{x}^-(t) &= A\hat{x}(t-1) + Bu(t-1) \\ \hat{x}(t) &= \hat{x}^-(t) + K(t)\left(y(t) - C\hat{x}^-(t)\right) \end{aligned} \tag{22}$$

$$\begin{aligned} P^-(t) &= AP(t-1)A^T + Q, \;\; P(0) = M \\ K(t) &= P^-(t)C^T\left(CP^-(t)C^T + N\right)^{-1} \\ P(t) &= (I - K(t)C)P^-(t) \end{aligned} \tag{23}$$

Remark. In the stochastic setting M, N, and Q represent the matrix inverses of the prior covariance matrices associated to the initial conditions, state and output noise respectively.

Notice that the recursive equation for $P(t)$ does not depend on the measurements, it only depends on A, C and the weighting matrices M, N, and Q .

3.4. Convergence

Firstly the convergence of the observer is addressed. The observer error dynamic is given by

$$e(t+1) = (A + KC)e(t) \tag{24}$$

where $e(t) = x(t) - \hat{x}(t)$. If the module of all eigenvalues of $A + KC$ are less than one, then the error will asymptotically converge to zero; i.e. $\lim_{t\to\infty} e(t) = 0$. Observability plays a fundamental role in the design of the observer gain K as stated in the following theorem.

Theorem. *[5] If the system (12) is observable it is always possible to find a matrix* $K \in R^{n\times Ml}$ *such that the the module of the eigenvalues of* $A + KC$ *will be less than one.*

For optimal design; i.e. an observer gain defined by (19) and (20), it is possible to state the following result:

Theorem. *[34] If there exists a positive definite and symmetric matrix P so that it is a solution of (20) and the observer gain is given by (19), then the error dynamic will be asymptotically stable.*

The proof considers the following positive definite function $V(e) = e^T Pe$. If P is a solution of (20) and the observer gain is given by (19), then $\Delta V(t) = V(t) - V(t-1) < -e(t)^T Qe(t) + (e(t+1) - e(t))^T R(e(t+1) - e(t))$. Thus, $\lim_{t\to\infty} V(t) = 0$ and therefore $\lim_{t\to\infty} e(t) = 0$.

The conditions for the convergence of the Kalman filter gain $K(t)$ and the time variant $P(t)$ matrix, defined by the recursive equation (23), are summarized in the following theorem

Theorem. *[34] Let $Q = ZZ^T$. Suppose that (A,Z) is reachable and (A, C) is observable, then*

$$P(t) \to P, \quad K(t) \to K, \quad \text{as } t \to \infty \tag{25}$$

these limiting equations are the only solutions of equations (20) and (19).

Detailed analysis of convergence issues can be found in [12] and [1]. If the pair given by A and Z is not reachable, this means that some elements of the error vector will not be affected by the filter corrective actions, and therefore the observations will not be able to reduce the estimation errors. In practice, Q must be always chosen as a full rank matrix in order to avoid the lack of reachability.

Remark. If the approximation error is not negligible; i.e. the states are far away from the linearizing point x_0, then the observer error will be bounded, but the error dynamic will not converge to zero. Let us consider a perturbed system given by

$$e(t+1) = (A + KC)e(t) + K\delta\big(x(t), x_0\big) \tag{26}$$

where x_0 is the linearizing point and $\delta(x(t), x_0)$ the higher order terms of the Taylor expansion. If the approximation term is bounded; i.e. $\| \delta(x(t), x_0) \| \leqslant \Delta$, the error can be bounded by

$$\| e(t) \| < \| (A + KC)^t e(0) \| + \| \sum_{j=0}^{t} (A + KC)^{t-k} K\delta\big(x(j), x_0\big) \|. \tag{27}$$

A final bound α_e; i.e. $\lim_{t\to\infty} \| e(t) \| = \alpha_e$ can be estimated as follows

$$\alpha_e < \frac{1}{1 - \lambda_{max}} \| K \| \Delta \tag{28}$$

where λ_{max} is the largest eigenvalue of $A + KC$.

4. Regularized observer

In certain EIT applications a simple random-walk model can be used to estimate the resistivity field. In this case the state space model is defined as

$$\begin{aligned} x(t+1) &= x(t) + \omega(t) \\ y(t) &= Cx(t) + \nu(t) \end{aligned} \tag{29}$$

where $x(0) = x_0$ is unknown. Since $A = I$ the observability matrix depends only on C; i.e. $\mathcal{O} = [C]$. Thus the inverse problem described by only the error associated to the observation

equation (29) is ill-posed, since the observability matrix is rank deficient since in practice $n > Ml$. In order to make the system observable it is possible to modify the observation model by either transforming the output or adding further p measurements. In this case, the number of extra outputs must be such that the observability matrix $\mathcal{O}$ must have rank n; i.e. a necessary condition is $n \leqslant Ml + p$.

4.1. Observability and convergence

There are two options to define the augmented output. The first option, proposed in [14], considers augmenting the output by some fictitious output

$$\tilde{y}_1 = \begin{bmatrix} \sqrt{R}y \\ \sqrt{S}L\bar{x} \end{bmatrix}, \quad \tilde{C}_1 = \begin{bmatrix} \sqrt{R}C \\ \sqrt{S}L \end{bmatrix} \tag{30}$$

where $\bar{x}$ is some a priori target value for x , $L \in R^{n\times n}$ is a regularization operator, R and S are positive definite and symmetric weighting matrices. This definition is motivated by the regularized solution given by the following functional

$$F(x) = \|y - Cx\|_R^2 + \|L(\bar{x} - x)\|_S^2 = \left\| \begin{bmatrix} \sqrt{R}y \\ \sqrt{S}L\bar{x} \end{bmatrix} - \begin{bmatrix} \sqrt{R}C \\ \sqrt{S}L \end{bmatrix} x \right\|^2 \tag{31}$$

The observability matrix is then an $Ml + n$ by n matrix $\mathcal{O} = \begin{bmatrix} \sqrt{R}C \\ \sqrt{S}L \end{bmatrix}$.

Remark. Additional observability measures, such as the ones based on Gramians [2] or in singular value decomposition of the information matrix [8], can be used not only to test if a given regularization strategy will provide the required conditions for the existence of a given K, and therefore the convergence of the observer, but also to analyze the observability of both the system and its subspaces under different regularization strategies.

The observer has the following structure

$$\hat{x}(t+1) = \hat{x}(t) + K^1\left(\tilde{y}_1(t) - \tilde{C}_1\hat{x}(t)\right) \tag{32}$$

where $K^1 \in R^{n\times Ml+n}$ is the observer gain. The estimation error is defined by $e(k) = x_0 - \hat{x}(k)$; where x_0 is the real state. Thus the error dynamic can be written as:

$$e(t+1) = \left(I + K^1\tilde{C}_1\right)e(k) + K^1\begin{bmatrix} 0 \\ \sqrt{S}L(\bar{x} - x_0) \end{bmatrix} \tag{33}$$

The second term in (33) may introduce a systematic error (bias) in the estimate. If the gain K^1 is designed such that the observer is asymptotically stable, then as $t \to \infty$, $\hat{e}(t+1) - \hat{e}(t) \to 0$, and the steady state solution of (33) will correspond to

$$K^1\begin{bmatrix} \sqrt{R}y - \sqrt{R}Cx^{ss} \\ \sqrt{S}L\left(\bar{x} - x^{ss}\right) \end{bmatrix} = 0 \tag{34}$$

where x^{ss} is the steady state solution.

The second option defines the output so that the necessary conditions for optimality are satisfied. Taking the first derivative of $F(x)$ and setting to zero

$$C^T R(y - Cx) + L^T SL(\bar{x} - x) = 0 \tag{35}$$

the output map can be redefined leading to the following output equations

$$\begin{aligned} \tilde{y}_2 &= C^T Ry + L^T SL\bar{x} \\ \tilde{C}_2 &= C^T RC + L^T SL \end{aligned} \tag{36}$$

The observability matrix is now a square matrix $\mathcal{O} = C^T RC + L^T SL$, which must be full rank. It is interesting to note that in this case, the existence of a unique solution implies also the observability of x. The error dynamic is

$$e(t+1) = \left(I + K^2\tilde{C}_2\right)e(k) + K^2\left[L^T\sqrt{S}L(\bar{x} - x_0)\right] \tag{37}$$

where $K^2 \in R^{n\times n}$ is the observer gain. If K^2 is designed such that such that the observer is asymptotically stable, then the steady state solution of (37) will satisfy

$$K^2\left[C^T R\left(Cx_0 - Cx^{ss}\right) + L^T SL\left(\bar{x} - x^{ss}\right)\right] = 0. \tag{38}$$

In this case, given that K^2 is a full rank matrix implies that there is a unique solution, x^{ss}, and this one will be the regularized solution.

An observer based on (36) is precisely the gradient algorithm associated to the minimization of (31), where the observer gain must be a positive definite matrix K^2 since (31) is convex; i.e. its Hessian is positive definite.

This option not only provides an observer with fewer parameters, since the gain matrix is just a square matrix of order n compared with the n by $n + Ml$ matrix of the first option, but also provides a direct link between the solution of the optimization problem and the associated characteristics of the observer.

Remark. For the observer based on (30), the gain matrix is not square and can be partitioned as $K^1 = [K_1^1 K_2^1]$. After some algebraic manipulations, it can be shown that the observer based on (30) will be equivalent to the one obtained using (36) if the observer gains are selected as

$$K_1^1 = K^2 C^T\sqrt{R}, \quad K_2^1 = K^2 L^T\sqrt{S}. \tag{39}$$

4.2. Optimal design

The cost function associated to the optimal design is given now in terms of matrix $\tilde{C}$ and output $\tilde{y}$, embedding in this way the spatial regularization in the observer design. For the fictitious outputs defined by (30) and $N^{-1} = I$, the cost function (21) leads to

$$\begin{aligned} I(t) = \frac{1}{2}\|x(0) - \hat{x}(0)\|^2_{M^{-1}} + \frac{1}{2}\Bigg[\sum_{k=0}^{t}\|y - C\hat{x}(k)\|^2_R + \|L\bar{x} - L\hat{x}(k)\|^2_S \\ + \|\hat{x}(k+1) - \hat{x}(k)\|^2_{Q^{-1}}\Bigg] \end{aligned} \tag{40}$$

as can bee seen in (40) the spatial regularization is taken into account in its third term. Unfortunately, this function is not well posed since it is unbounded as t tends to infinity, even if the observer converges. For a finite horizon, the problem can be solved using efficient numerical algorithms as described in [23]. A bounded cost function can be obtained by subtracting the optimal solution ; i.e. $F(x^{ss})$,

$$I(t) = \frac{1}{2}\| x(0) - \hat{x}(0) \|^2_{M^{-1}} + \frac{1}{2}\left[\sum_{k=0}^{t} F\left(\hat{x}(k)\right) - F\left(x^{ss}\right) + \| \hat{x}(k+1) - \hat{x}(k) \|^2_{Q^{-1}} \right]. \quad (41)$$

By using the fictitious outputs defined by (36) in (21), the minimized functional can be written as

$$\begin{aligned} I(t) = & \frac{1}{2}\| x(0) - \hat{x}(0) \|^2_{M^{-1}} \\ & + \frac{1}{2}\left[\sum_{k=0}^{t} \| C^T R y + L^T S L \bar{x} - \left(C^T R C + L^T S L \right) \hat{x}(k) \|^2_{N^{-1}} \right. \\ & \left. + \| \hat{x}(k+1) - \hat{x}(k) \|^2_{Q^{-1}} \right] \end{aligned} \quad (42)$$

The cost function (42) represents a well posed cost function for dynamic regularization; i.e. it is bounded if the observer converges.

The observer gain design can be carried out either by using the steady state solution provided by (20) or using the recursive equation (23).

5. Simulated examples

As an illustrative EIT example a circular domain with 16 electrodes uniformly distributed is considered. In order to solve the forward model and the simulated voltages a mesh of 2714 elements and 1447 nodes was used, as depicted in figure 1(a). In the inverse computations a mesh of 480 elements and 281 nodes, as seen in figure 1(b), was considered in order to reduce the number of variables to be estimated and to avoid the inverse crime.

The regularization matrix L is a sparse matrix with a row for each element in the mesh. Every row of L has nonzero elements equal to 1 in the columns associated to neighboring elements of i, and $-n_i$ in the column i; where n_i is the number of neighboring elements. This corresponds to the prior assumption of a homogenous field. A total of 256 measured outputs, corresponding to 16 injection patterns, will be considered.

An observer and three different Kalman filters will be simulated. The observer is based on (18), (19) and (20) with $y = \tilde{y}_2$ and $C = \tilde{C}_2$. The linearized Kalman filter (LKF) is based on equations (22) and (23). The regularized version with option 1 (RLKF1) considers $y = \tilde{y}_1$ and $C = \tilde{C}_1$, and Regularized LKF with option 2 (RLKF2) considers $y = \tilde{y}_2$ and $C = \tilde{C}_2$.

It is worth pointing out that the speed of convergence must be balanced against process and measurement noise by tuning the weighting matrices Q, R and N. In order to illustrate the effect of both N and S, they are assumed diagonal matrices defined as $\gamma_v I$ and $\gamma_s I$ respectively, where γ_v and γ_s are scalar weighting factors. table 2 summarizes the parameters used to calculate the eigenvalues of $A + KC$ for different values of γ_v and γ_s. The calculations considered the matrix A as the identity matrix and C as $\tilde{C}_1$ for standard regularization and $\tilde{C}_2$ for the proposed one. As seen in figure 2, for both regularization approaches, increasing γ_v increases the value of the largest eigenvalue; i.e. the speed of convergence decreases. On the other hand, if γ_s increases the speed of convergence also increases.

One of the key issues in real-time operations is the number of floating point operations (FLOPs) required to update the estimates. The following FLOP estimates are obtained by considering an LU factorization to carry out the inverse of a matrix [9]. The number of FLOPs required for a constant gain observer is given by

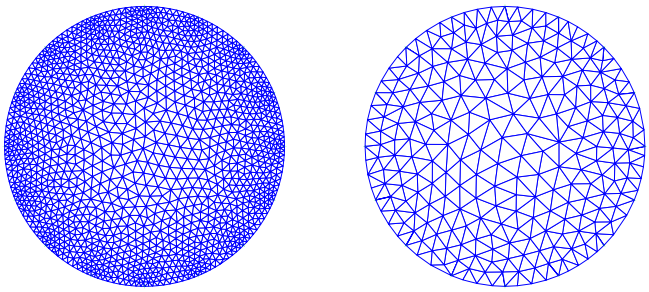

(a) Direct problem (b) Inverse problem

Figure 1. FEM meshes.

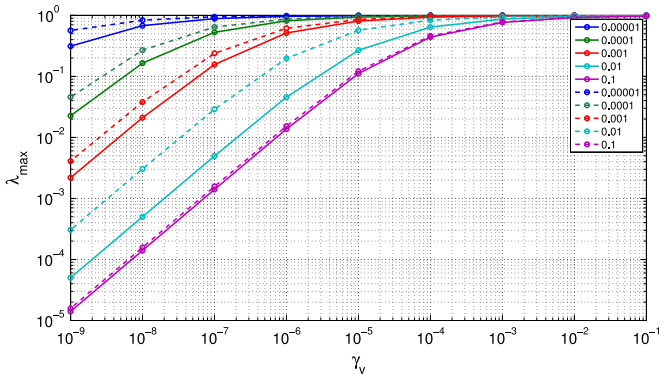

Figure 2. Module of the largest eigenvalue of $A + KC$ for the standard regularization (solid line) and proposed approach (dashed line) for different values of γ_v and γ_s.

Table 1. Number of floating points operations for $n = 430, m = 1, Ml = 256$.

Algorithm	p	*FLOPS*
LKF	256	$9.9606\ 10^8$
RLKF1	686	$2.6605\ 10^9$
RLKF2	430	$1.5489\ \ 10^9$
OBS	430	$1.8734\ \ 10^6$

Table 2. Parameters of the different algorithms.

Algorithm	S	R	N	Q	$P(0)$
LKF	-	-	$\gamma_v I$	$10\ I$	$10^4\ I$
RLKF1	$\gamma_s I$	I	$\gamma_v I$	$10\ I$	$10^4\ I$
RLKF2	$\gamma_s I$	I	$C^T\gamma_v IC$	$10\ I$	$10^4\ I$
OBS	$\gamma_s I$	I	$C^T\gamma_v IC$	$10\ I$	$10^4\ I$

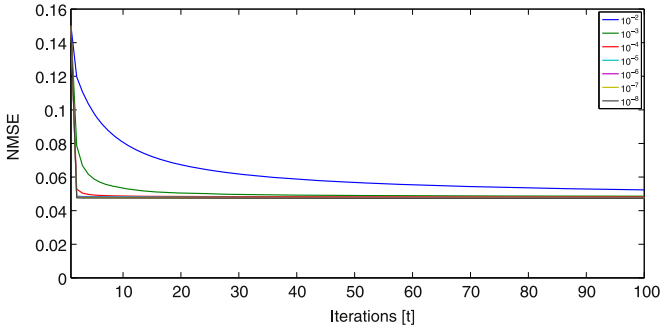

(a) LKF

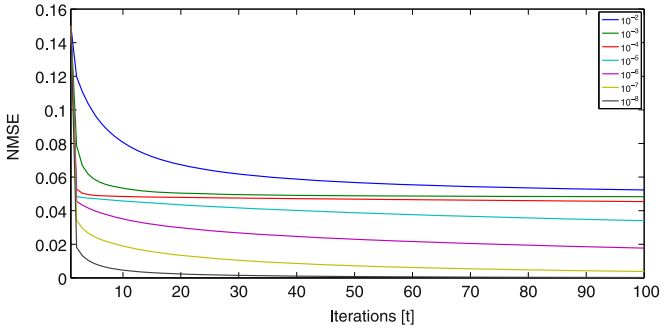

(b) RLKF1

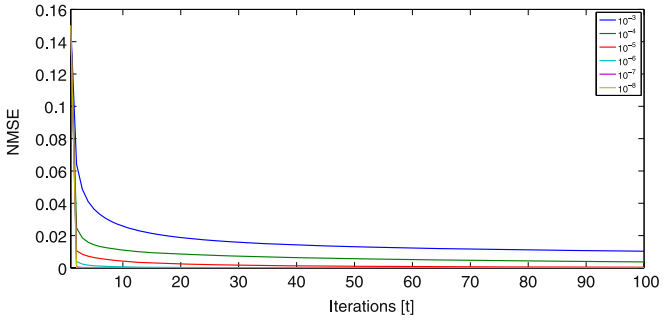

(c) RLKF2

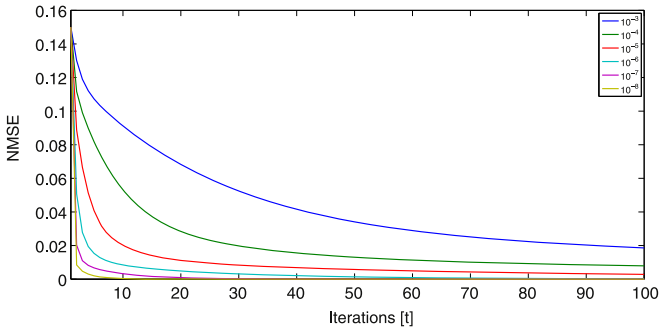

(d) Fixed gain observer

Figure 3. Homogeneous field: normalized mean square errors (NMSEs) of the estimates for different γ_v.

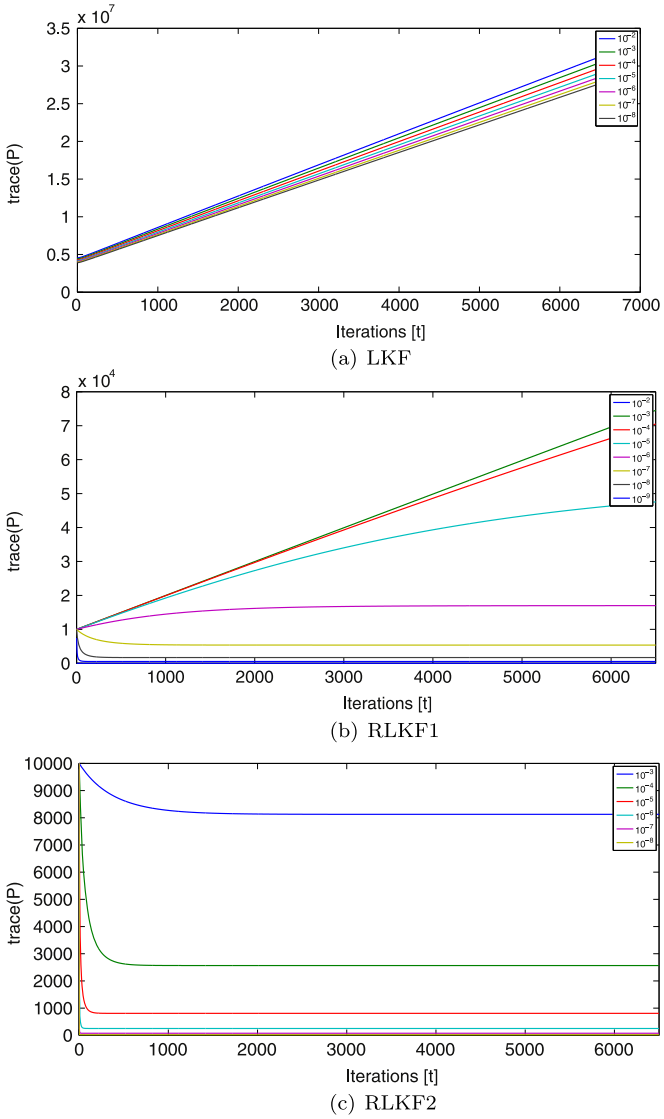

Figure 4. Homogeneous field: trace of the $P(t)$ matrices P for different γ_v.

$$FLOPS_{Obs} = 2n^2 + 4np + 2mn - 3n, \tag{43}$$

and for Kalman filters

$$FLOPS_{KF} = 6n^3 + 2p^3 + \frac{3p^2}{2} + 2mn + 2np + 2np^2 + 4n^2p - \frac{5p}{6} - 2n - n^2, \tag{44}$$

where n is the number of states, m number of inputs and p is the number of outputs. The number FLOPs for a Kalman filter depends on p^3, while for the observer it is just proportional to p. Since the number of states and inputs are the same for all the algorithms, the number of FLOPs required to accomplish one iteration is defined by the number of outputs, as summarized in table 1. As seen in this table, the recursive algorithms require three order of

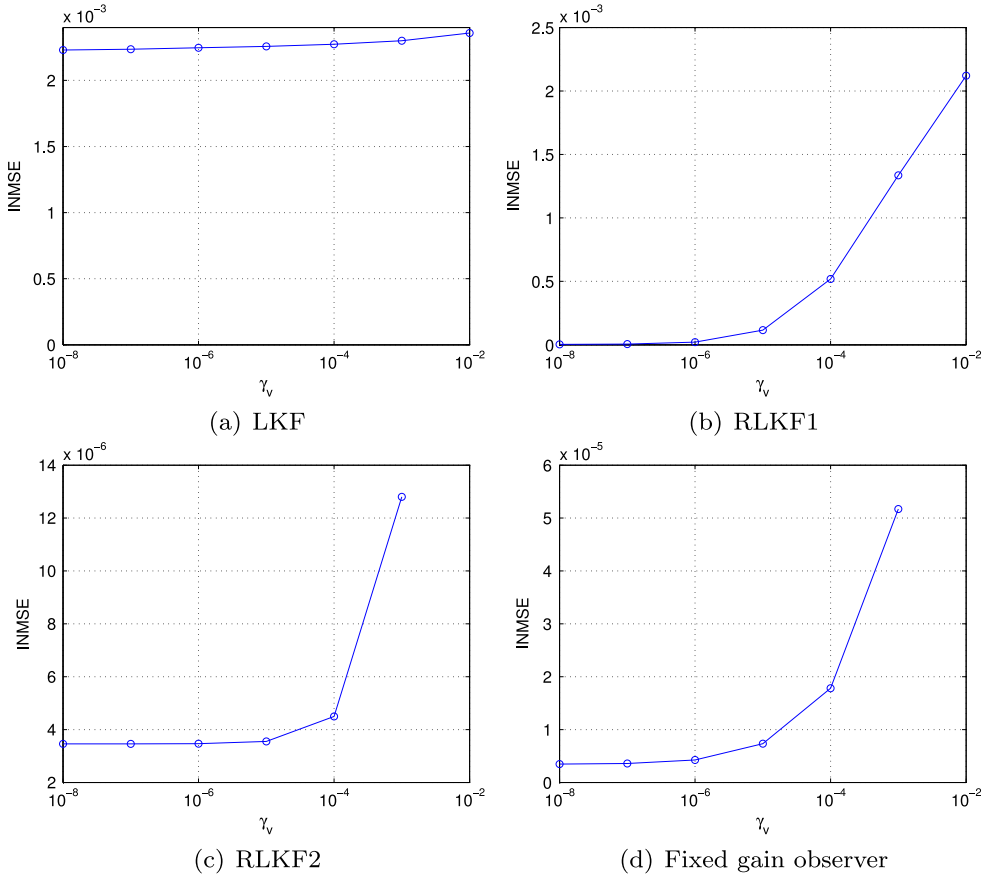

Figure 5. Homogeneous field: Integrated NMSE for different γ_v.

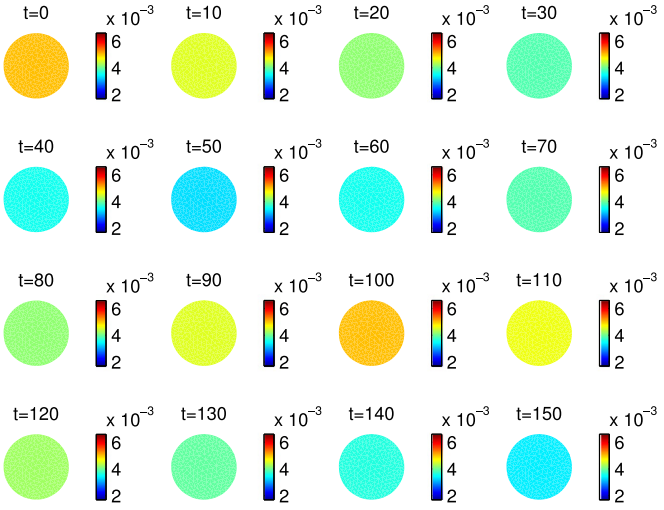

Figure 6. Time-varying homogenous conductivity field.

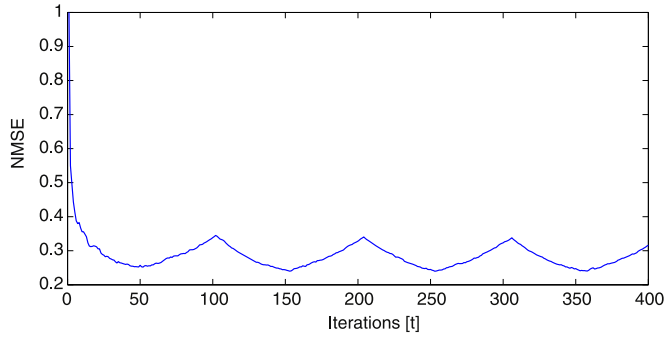

(a) Normalized mean squared error

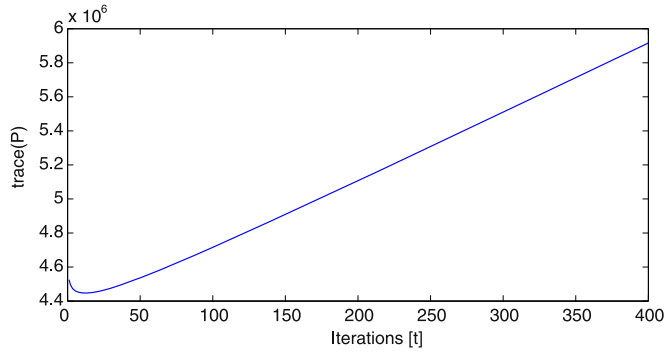

(b) Trace of $P(t)$ matrix

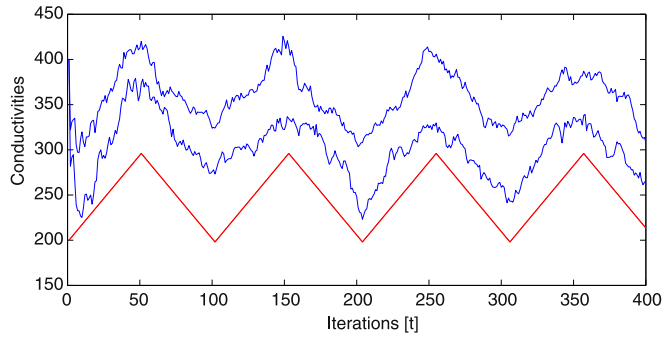

(c) Estimated variables (blue), real values (red)

Figure 7. Time-varying homogenous resistivity field estimation by means of LKF.

magnitude more FLOPs than the simple observer. It is also worth pointing out that the proposed regularization approach; i.e. option 2, also requires 40% less FLOPS than the conventional approach.

The normalized mean squared error (NMSE) and the integral of the NMSE, over a time interval T, defined as follows:

$$NMSE\,(t) = \int_{\Omega} \left(\frac{\hat{\rho}\,(t) - \rho_0}{\rho_0} \right)^2 \mathrm{d}s \tag{45}$$

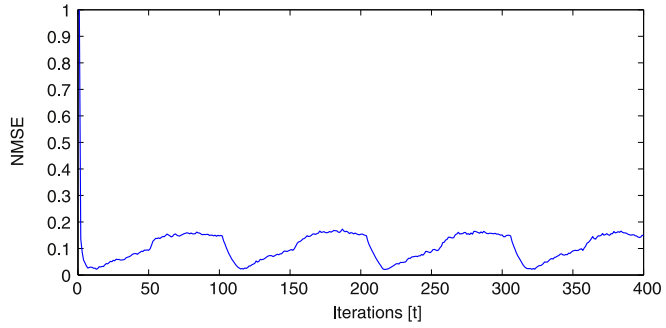

(a) Normalized mean squared error

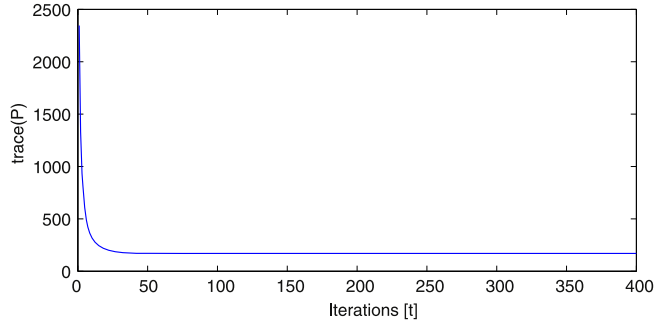

(b) Trace of $P(t)$ matrix

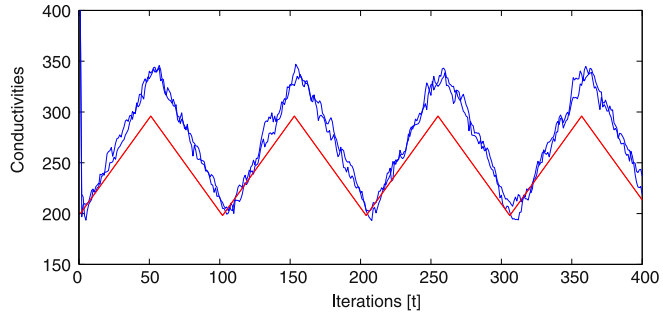

(c) Estimated variables (blue), real values (red)

Figure 8. Time-varying homogenous resistivity field estimation by means of RLKF1.

$$INMSE = \frac{1}{T}\int_0^T NMSE\,(t)\mathrm{d}t \tag{46}$$

will be calculated for each experiment in order to compare their performance.

The first set of experiments considers a homogenous resistivity field with $\rho = 200$ and measurements without noise. The initial conditions for all the algorithms are $\hat{\rho}\,(0) = 230$ and the different parameters for each of them are summarized in table 2. The regularization term was selected as $\gamma_s = 10^{-3}$. In order to illustrate the effect of weighting matrix N, different values of γ_v were considered.

The evolution of the NMSE is shown in figure 3 for different values of γ_v. As seen in this figure all four algorithms have asymptotic convergence. The speed of convergence depends on γ_v, smaller values of γ_v mean faster convergences. The regularized algorithms reach smaller

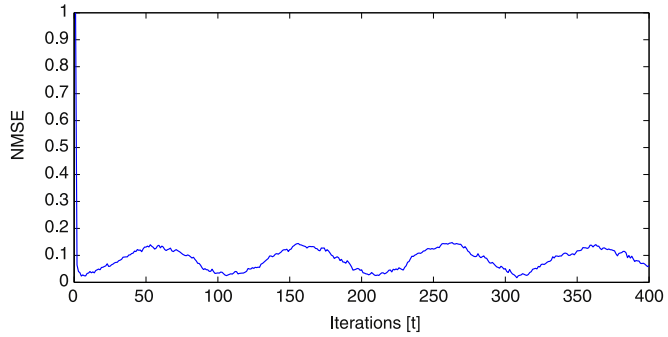

(a) Normalized mean squared error

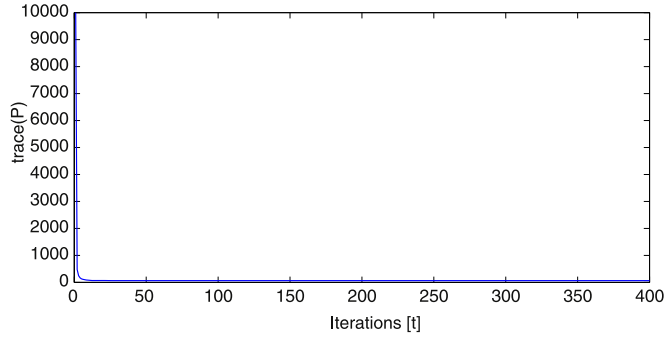

(b) Trace of $P(t)$ matrix

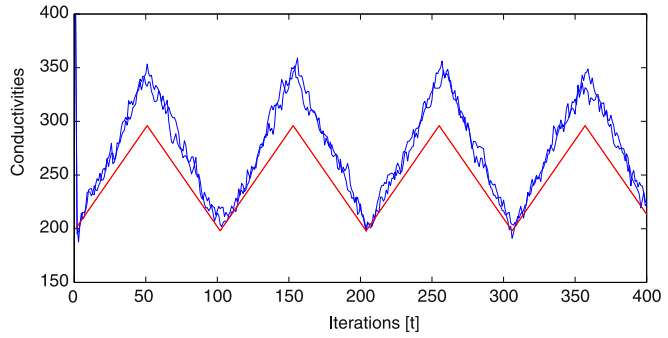

(c) Estimated variables (blue), real values (red)

Figure 9. Time-varying homogenous resistivity field estimation by means of RLKF2.

NMSE values compared with the plain LKF. It is interesting to note that for a given γ_v, RLKF2 converges faster than the constant gain observer.

The long term evolution of the $P(t)$ matrices in terms of their traces are given in figure 4. The trace, in this case, provides an idea about the evolution of the diagonal values of $P(t)$. As it can clearly be seen for LKF, the trace of the $P(t)$ matrix blows-out, while the ones associated to the regularized filters are bounded. This result is a direct consequence of the lack of observability associated to the model used by LKF.

The integral of the NMSE for the different algorithms are depicted in figure 5, as seen in these figures as γ_v decreases, the INMSE will decrease up to reach a small final value. The smallest final value was obtained by RLKF2.

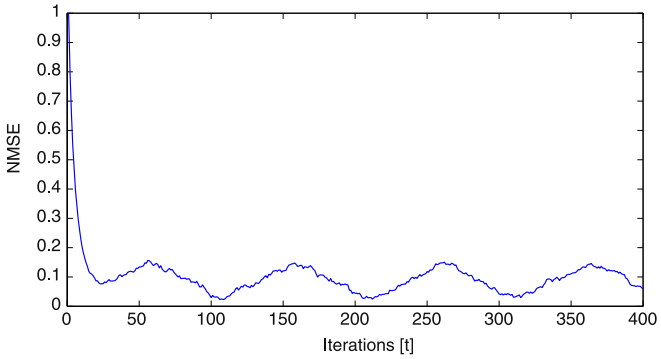

(a) Normalized mean squared error

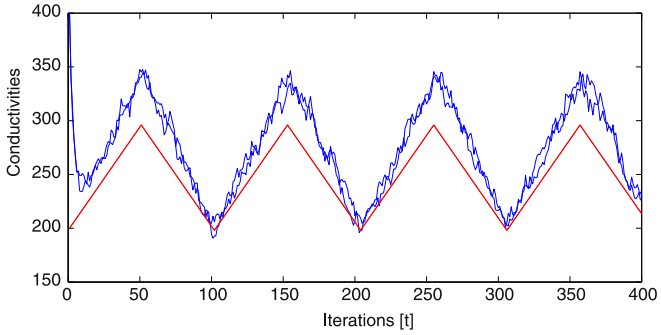

(b) Estimated variables

Figure 10. Time-varying homogenous resistivity field estimation by means of OBS.

The second set of experiments considers a homogenous conductivity field driven by an external signal $u(t)$ through the following dynamics

$$\rho(t+1)^{-1} = \rho(t)^{-1} + u(t) \tag{47}$$

The external signal $u(t)$ is a periodic square pulse signal having a period of 100 samples. The time-evolution of the conductivity field has a triangular form, as seen in figure 6, due to the assumed dynamic, equation (47). All the algorithms were simulated by considering the same weighting matrices with $\gamma_v = 10^{-3}$ and $\gamma_s = 10^{-2}$, and a measurement noise with an amplitude of about 5% of the measured voltages values.

The NMSE, $P(t)$ matrix and some estimated variables obtained by LKF are shown in figure 7. Figure 7(a) shows that the NMSE decreases fast and is kept bounded; this residual error is due to the fact that the observer has been designed by using an approximation around a linearizing point. As in the previous examples, the model used by LKF does not satisfy the observability condition and therefore the boundedness of the $P(t)$ matrix cannot be ensured, as seen in figure 7(b). Figure 7(c) shows the estimation of resistivities at two different locations, as seen in the figure none of them approach the real values, which are depicted in red.

The regularized RLKF1 provides better estimates in terms of NMSE than LKF, as seen in figure 8(a). The $P(t)$ matrix is bounded as expected, figure 8(b). The difference between the estimated resistivity values and the real ones is smaller than the one obtained by LKF, and at the linearization point is very small, as shown in figure 8(c).

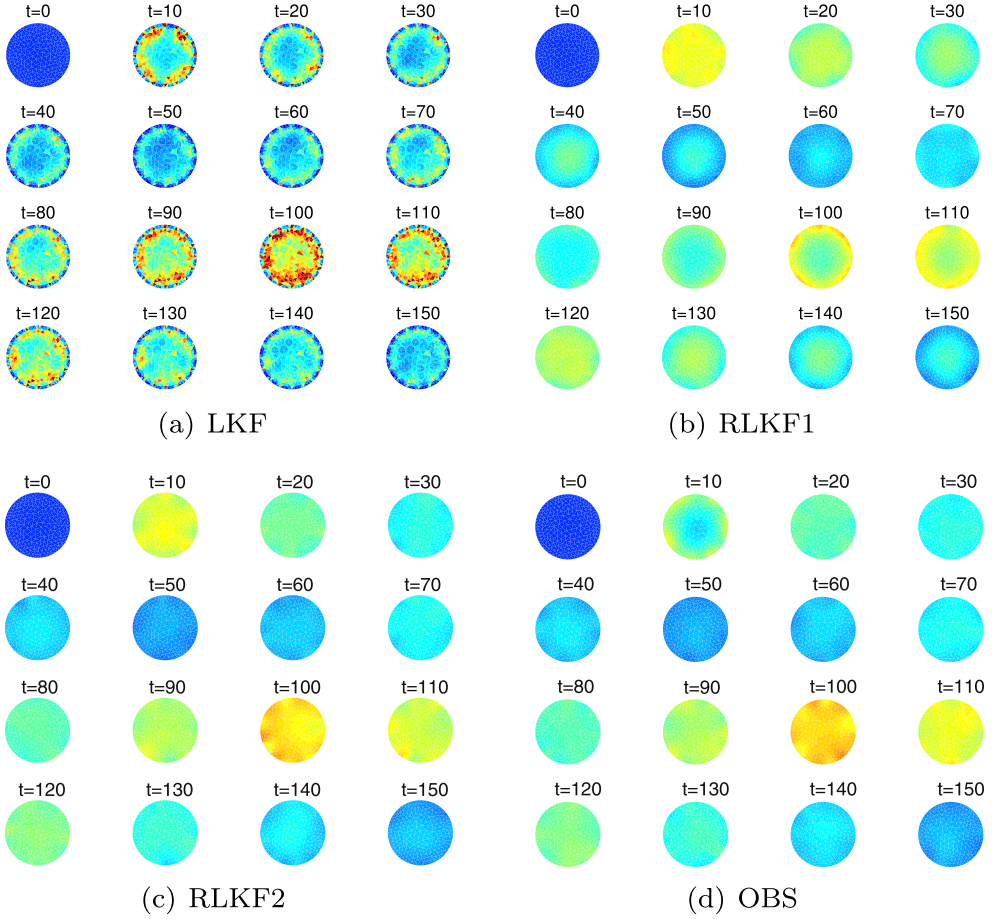

Figure 11. Snapshots of the estimated time-variant homogenous field.

The regularized RLKF2 provides even better estimates in terms of NMSE than LKF and RLKF1, as seen in figure 9(a). The $P(t)$ matrix is also bounded as seen in figure 9(b). The estimated values of the resistivity are closer to the real ones matching them at the linearizing point, as shown in figure 9(c).

For the same set of parameter used for RLKF2, the observer has similar steady state behavior, but slower convergence speed, as seen in figures 10(a) and (b). Figure 10(b) also shows that the difference between the estimated resistivity values tends to zero. In addition, the difference between the estimated resistivity values and the real ones converge to zero at the linearizing point.

Different snapshots of the estimated field show high spatial variability for the LKF, as as seen in figure 11(a). However, for RLKF1 the difference between the estimated values has been decreased; which means an improved spatial smoothness of the estimated field, as depicted in figure 11(b). For both RLKF2 and OBS the smoothness constraint has been effectively enforced by the use of the regularization as seen in figures 11(c) and (d) respectively.

The third set of experiments considers a circular object within a homogeneous field and measurements without noise, as shown in figure 12.

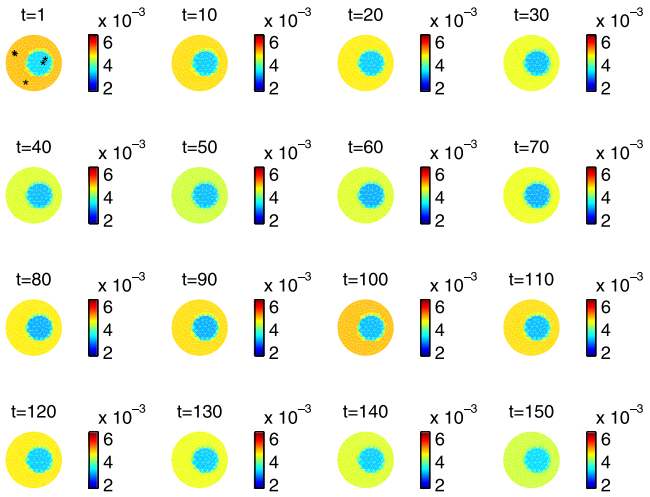

Figure 12. Inhomogeneous resistivity field.

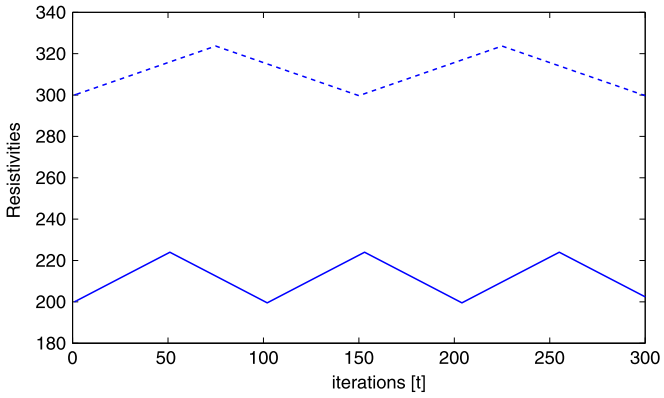

Figure 13. Evolutions of the resistivities: background (continuous), circular object (dashed).

The time variations of the background and object resistivities are periodic with periods of 100 and 150 samples respectively, as shown in figure 13.

A small regularization term, i..e. $\gamma_s = 5\ 10^{-5}$, is considered since the prior assumption does not completely match the real spatial variations, and therefore some bias in the estimates is expected. The linearization was carried out using a homogenous resistivity field with $\rho = 200$. As commented in section 3.4., this fact introduces some errors in the observation model, which only affect the final error but not the stability of the algorithms. In this example, as the resistivities vary independently, the standard random walk model; i.e. without inputs, was assumed for describing their dynamics. This example also shows that it is possible to estimate time-varying conductivities even though we do not measure the inputs.

The NMSE, $P(t)$ matrix and some estimated variables obtained by LKF are shown in figure 14. The NMSE decreases fast and is kept bounded, as seen in figure 14(a). The

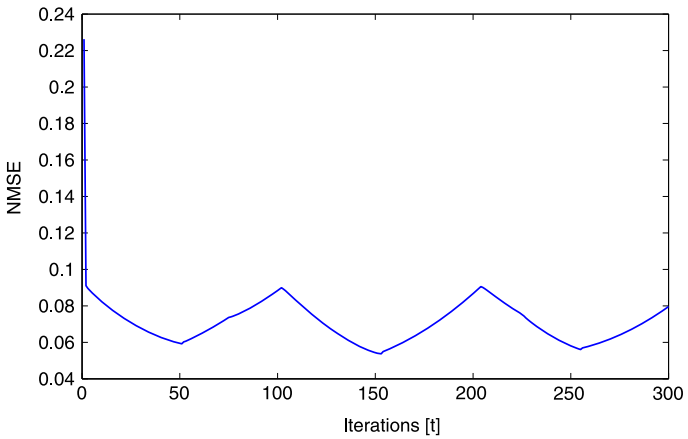

(a) Normalized mean squared error

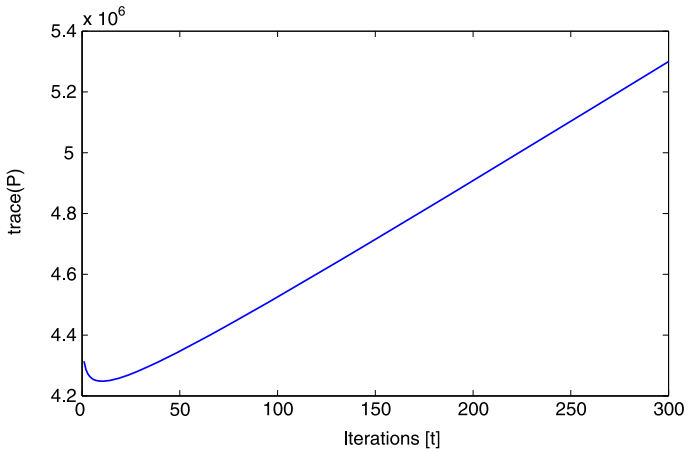

(b) Trace of $P(t)$ matrix

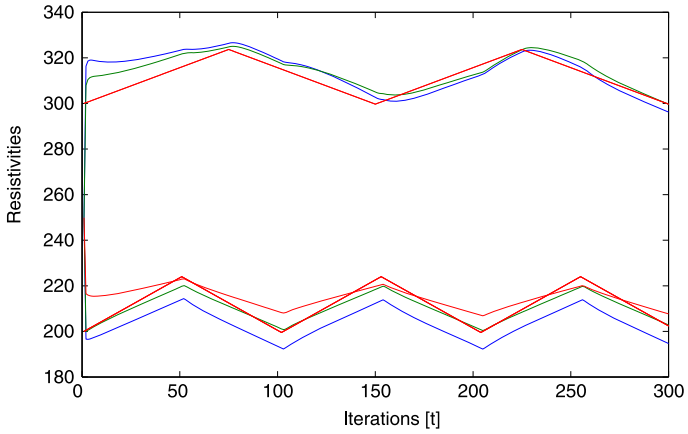

(c) Estimated variables (blue), real values (red)

Figure 14. Object and background resistivity estimation by means of LKF.

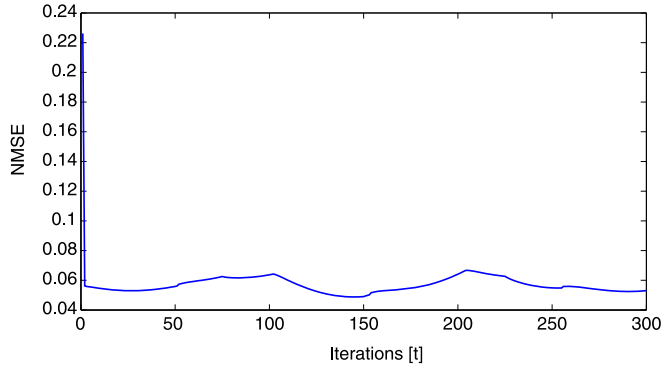

(a) Normalized mean squared error

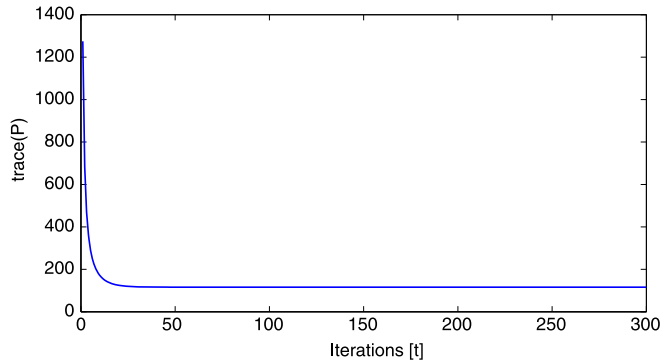

(b) Trace of $P(t)$ matrix

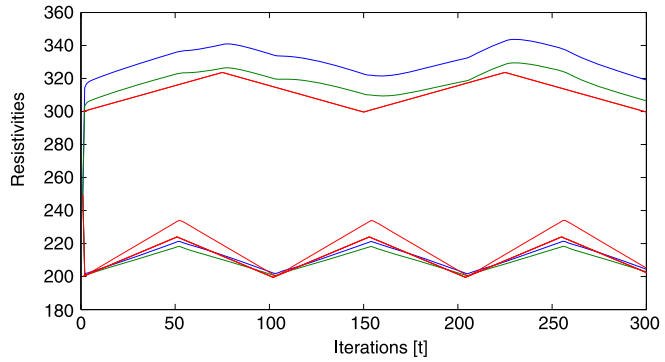

(c) Estimated variables (blue,green, light red), real values (red)

Figure 15. Object and background resistivity estimation by means of RLKF1.

evolution of $P(t)$ in figure 14(b) shows a linear growth. Figure 14(c) shows the estimation of resistivities at different locations, as seen in the figure the estimated resistivities of the object converge near to the real values, but the estimates of the background remain far away from the real values. This means that the estimated homogenous field has high spatial variability, as seen in figure 18(a). The fact that LKF can provide reasonable estimates in a finite time for ill-conditioned problems is not a surprise, since early stopping provides some kind of regularization that can also be used for obtaining regularized solutions as described in [21] .

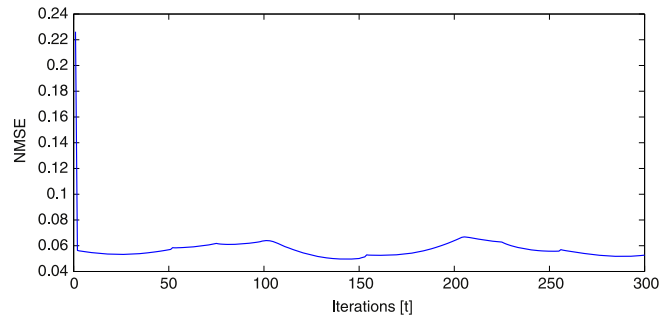

(a) Normalized mean squared error

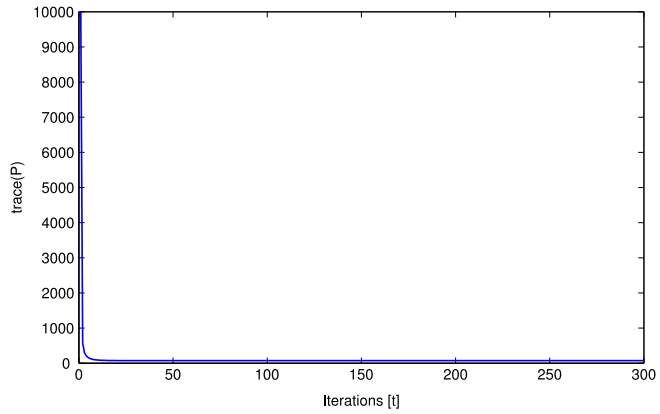

(b) Trace of $P(t)$ matrix

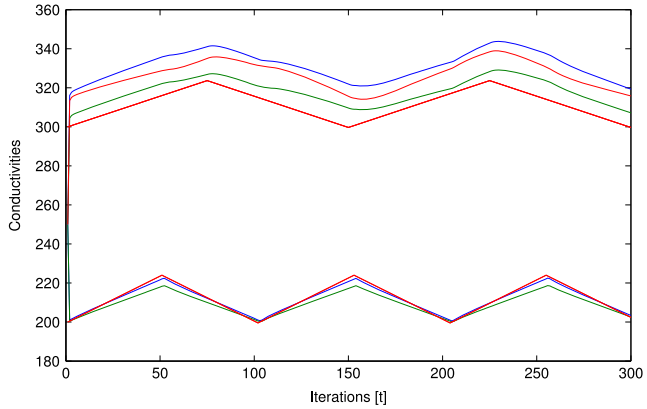

(c) Estimated variables (blue,green, light red), real values (red)

Figure 16. Object and background resistivity estimation by means of RLKF2.

The regularized RLKF1 provides better estimates in terms of NMSE than LKF, as seen in figure 15(a). The $P(t)$ matrix is bounded as expected, see figure 15(b). The difference between the estimated resistivity values and the real ones for the object are bigger than the one obtained by LKF. However, the differences for the background resistivities are smaller and at the linearization point are very small, as shown in figure 15(c). Better estimates of the homogenous field also means a less spatial variation of the estimated field. The overall performance, in terms of the NMSE, is better than the LKF.

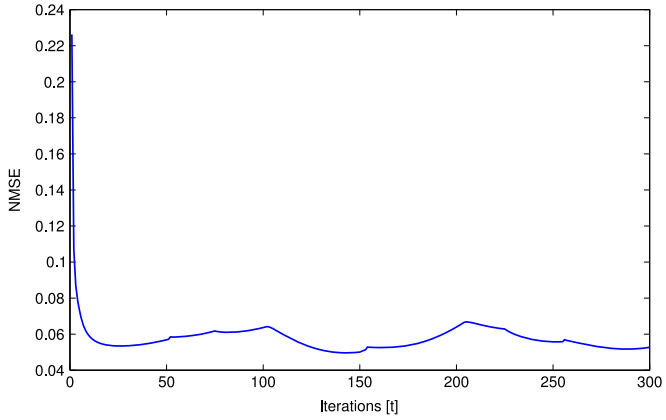

(a) Normalized mean squared error

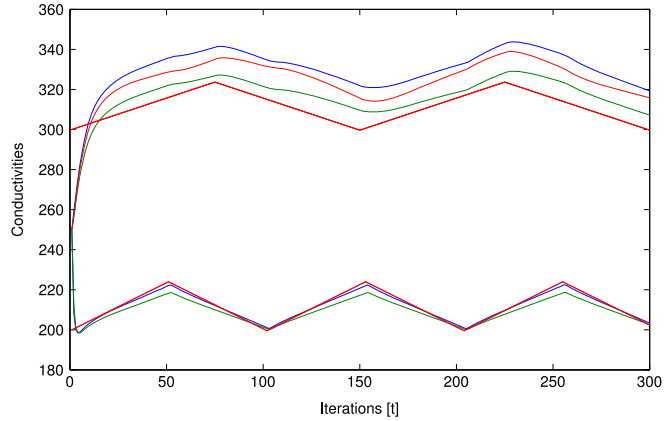

(b) Estimated variables (blue,green, light red), real values (red)

Figure 17. Object and background resistivity estimation by means of OBS.

The RLKF2 provides smaller NME values compared with RLK1, as seen in figure 16(a). Figure 16(b) also shows that the difference between the estimated resistivity values tends to zero at the linearization point, but the estimation errors are bigger far away from this point.

For the same set of parameter used for RLKF2, the observer has similar steady state behavior, but slower convergence speed, as seen in figures 17(a) and (b). It is worth pointing out that the use of an observer may be attractive when it is necessary to reach a compromise between a reduction on the number of calculations and transient performance.

Different snapshots of the estimated field obtained by LKF as depicted in figure 18(a) show that the estimated resistivities of the object converge near to the real values, but the estimates of the background remain far away from the real values. This means that the estimated homogenous field has high spatial variability. The use of regularization by RLKF1 enforces some smoothness on the conductivity field obtaining better estimates of the background as seen figure 18(b). The estimated field obtained by RLKF2, figure 18(c), is very similar to the one obtained by RLKF1. The estimates obtained by the observer show that the smoothness of the estimations has also been preserved, as seen in figure 18(d).

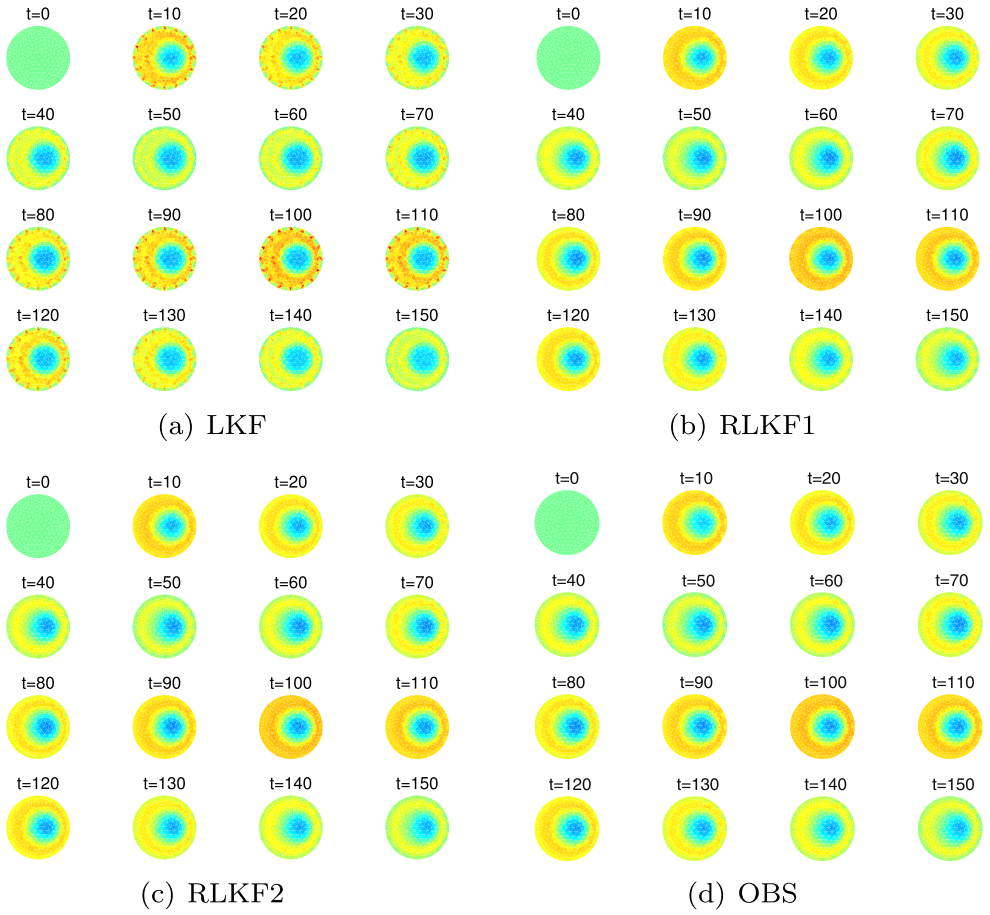

Figure 18. Snapshots of the estimated field.

6. Conclusions

In this paper we have analyzed the solution of an EIT inverse problem from the perspective of a dynamic estimation problem providing some insight about the relationship between system properties and the performance of estimation algorithms. The concept of observability plays a key role in solving the dynamic estimation problem since it ensures the existence of a solution. The results show that the lack of observability prevents the use of dynamic estimation algorithms in real-time, since under this condition it is not possible to obtain meaningful estimates, and also to ensure the boundedness of all the signals.

The design of estimation algorithms for EIT have traditionally considered the regularization of the inverse problem by the addition of extra outputs. The concept of observability not only validate this approach, but also extends its significance by taking into account the system dynamic and ensuring, in this way, the well-posedness of the estimation problem.

The interpretation in terms of observers enables the design of estimation algorithms with prescribed speed of convergence, low complexity in terms of the number of floating point operations, and similar performance compared to recursive estimation algorithms. In addition,

an alternative output definition for taking into account the regularization term in the observer structure has been proposed. This provides a direct connection between the existence of the regularized solution and the observability of the system, and it also enables the use of an infinite cost function to address optimal observer design. A key feature of this approach is the important reduction in terms of FLOPS compared to the traditional one. The extention of these results to reduce the estimation error by considering the nonlinear nature of the EIT inverse problem is part of our current research interest.

Acknowledgments

The support of Project Fondecyt 1130682, Fondap 15130015 and the Academy of Finland Project 250215, Finnish Centre of Excellence in Inverse Problems Research, are kindly acknowledged.

References

[1] Anderson B and Moore J B 2005 *Optimal Filtering* (*Dover Books on Electrical Engineering*) (Mineola, NY: Dover)
[2] Antsaklis P J and Michel A N 2006 *Linear systems* (Boston: Birkhauser)
[3] Besancon G 2007 *Nonlinear Observers and Applications* (*Lecture Notes in Control and Information Sciences* vol 363) (Berlin: Springer)
[4] Crassidis J L and Junkins J L 2012 *Optimal Estimation of Dynamic Systems* 2nd edn (Boca Raton, FL: CRC Press)
[5] Friedland B 2005 *Control System Design: An Introduction to State-Space Methods* (Mineola, NY: Dover)
[6] Gibbs B P 2010 *Advanced Kalman filtering, least-squares and modeling : a practical handbook* (Hoboken, NJ: John Wiley & Sons)
[7] Grewal M S and Andrews A P 2008 *Kalman Filtering: Theory and Practice Using MATLAB* (Hoboken, NJ: John Wiley & Sons)
[8] Hong S, Chun H H, Kwon S H and Lee M H 2008 Observability mesures and their application to GPS/INS *IEEE Transaction on Vehicular Technology* **57** 97–105
[9] Hunger R 2007 Floating point operations in matrix-vector calculus *Technical Report V.1.3* (Technische Universität München: Associate Institute for Signal Processing)
[10] Ijaz U Z, Chung S I, Khambampati A K, Kim K Y and Kim S 2008 Electrical resistance imaging of time varying interface in stratified flows using unscented Kalman filter *Meas. Sci. Technol.* **19** 065501
[11] Ijaz U Z, Khambampati A K, Lee J S, Kim S and Kim K Y 2008 Nonstationary phase boundary estimation in electrical impedance tomography using unscented Kalman filter *J. Comput. Phys.* **227** 7089–112
[12] Jazwinski A H 1970 *Stochastic Processes and Filtering Theory* (New York: Academic)
[13] Kailath T, Sayed A H and Hassibi B 2000 *Linear Estimation* (Englewood Cliffs, NJ: Prentice Hall)
[14] Kaipio J and Somersalo E 1999 Nonstationary inverse problems and state estimation *J. Inverse and Ill-posed Problems* **7** 273–82
[15] Khambampati A K, Rashid A, Ijaz U Z, Kim S, Soleimani M and Kim K Y 2009 Unscented Kalman filter approach to tracking a moving interfacial boundary in sedimentation process using three dimensional electrical impedance tomography *Phil. Trans. R. Soc. A* **367** 3095–120
[16] Kim B S, Kim K Y, Kao T J, Newell J C, Isaacson D and Saulnier G J 2006 Dynamic electrical impedance imaging of a chest phantom using the Kalman filter *Physiol. Meas.* **27** S81
[17] Kim K Y, Kang S I, Kim M C, Kim S, Lee Y J and Vauhkonen M 2003 Dynamic electrical impedance tomography with known internal structures *Inv. Prob. Eng.* **11** 1–19
[18] Kim K Y, Kim B S, Kim M C, Lee J L and Vauhkonen M 2001 Image reconstruction in time-varying electrical impedance tomography based on extended Kalman filter *Meas. Sci. Technol.* **12** 1032–9

[19] Kolehmainen V, Voutilainen A and Kaipio J P 2001 Estimation of non-stationary region boundaries in EIT–state estimation approach *Inverse Problems* **17** 1937
[20] Reilly J O' 1983 *Observers for Linear Systems* (*Mathematics in Science and Engineering* vol 170) (New York: Academic)
[21] Rosasco L, Tacchetti A and Villa S 2014 Regularization by early stopping for online learning algorithms arXiv:1405.0042v1 [stat.ML]
[22] Ruuskanen A R, Seppänen A, Duncan S, Somersalo E and Kaipio J P 2006 Using process tomography as a sensor for optimal control *Appl. Numer. Math.* **56** 37–54
[23] Schmitt U, Louis A K, Wolters C and Vauhkonen M 2002 Efficient algorithms for regularization of dynamic inverse problems: II applications *Inverse Problems* **18** 659–76
[24] Seppänen A, Vauhkonen M, Vauhkonen P J, Somersalo E and Kaipio J P 2001 State estimation with fluid dynamical evolution models in process tomography—an application to impedance tomography *Inverse Problems* **17** 467
[25] Seppanen A, Vauhkonen M, Vauhkonen P J, Voutilainen A and Kaipio J P 2008 State estimation in process tomography–three-dimensional impedance imaging of moving fluids *Int. J. Numer. Methods Eng.* **73** 1651–70
[26] Seppänen A, Voutilainen A and Kaipio J P 2009 State estimation in process tomography reconstruction of velocity fields using EIT *Inverse Problems* **25** 085009
[27] Simon D 2006 *Optimal State Estimation: Kalman, H_∞ and Nonlinear Approaches* (Hoboken, NJ: John Wiley & Sons)
[28] Soleimani M, Vauhkonen M, Yang W, Peyton A, Kim B S and Ma X 2007 Dynamic imaging in electrical capacitance tomography and electromagnetic induction tomography using kalman filter *Meas. Sci. Technol.* **18** 3287–94
[29] Sorenson H W 1970 Least squares estimation: from Gauss to Kalman *IEEE spectrum* **7** 63–8
[30] Trigo F C, Gonzalez-Lima R and Amato M B 2004 Electrical impedance tomography using the extended Kalman filter *IEEE Trans Biomed Eng* **51** 72–81
[31] Vauhkonen M, Karjalainen P A and Kaipio J P 1998 A Kalman filter approach to track fast impedance changes in electrical impedance tomography *IEEE Trans. Biomed. Eng.* **45** 486–93
[32] Vauhkonen M, Vadász D, Kaipio J P, Somersalo E and Karjalainen P A 1998 Tikhonov regularization and prior information in electrical impedance tomography *IEEE Trans. Medical Imaging* **17** 285–93
[33] Voutilainen A, Lehikoinen A, Vauhkonen M and Kaipio J P 2011 A reduced-order filtering approach for 3D dynamical electrical impedance tomography *Meas. Sci. Technol.* **22** 025504
[34] Walrand J and Dimakis A 2006 *Random Processes in Systems — Lecture Notes* (*Department of Electrical Engineering and Computer Sciences*) (Berkeley CA: University of California) 94720
[35] Yorkey T J, Webster J G and Tompkins W J 1987 Comparing reconstruction algorithms for Electrical Impedance Tomography *IEEE Trans. Biomed. Eng.* **34** 843–52
[36] Zifan A, Liatsis P and Chapman B E 2013 The use of the Kalman filter in the automated segmentation of EIT lung images *Physiol. Meas.* **34** 671–94